Robust Speed Control of Permanent Magnet Synchronous Motors Using Two-Degrees-of-Freedom Control

Fortino Mendoza-Mondragón, Víctor Manuel Hernández-Guzmán, and Juvenal Rodríguez-Reséndiz, *Senior Member, IEEE*

***Abstract*—In this paper, a two-degrees-of-freedom controller is proposed for robust speed regulation in permanent magnet synchronous motors (PMSM). Our proposal constitutes an extension of a control scheme previously introduced in the literature for permanent magnet brushed dc motors to the case of PMSM. We formally prove global exponential stability of the desired equilibrium point, and we take into account the nonlinear motor electric dynamics during the stability proof. Several experiments are presented, which verify that the closed-loop control system is robust with respect to parameter uncertainties and outstanding torque disturbance rejection is performed. These results are compared to those obtained with a standard proportional-integral speed control scheme. We conclude that good performance, simplicity, and easy controller commissioning in practice are significant advantages of our proposal, which render it suitable for the motor drive community.**

***Index Terms*—Field-oriented control (FOC), permanent magnet synchronous motor (PMSM), robustness, speed control, two-degree-of-freedom (2-DOF) control.**

I. Introduction

SPEED regulation of electric motors is an important requirement in many industrial applications such as robotics, computer numerical control, traction motors, air conditioning, pumps, etc. Recently, due to the need for higher efficiency and lower size, the use of the permanent magnet synchronous motors (PMSM) has been growing and replacing the induction motor in applications such as electric vehicles and home appliances [1], [2]. The main disadvantage of PMSM is that its model is nonlinear, which complicates the controller design task. This drawback has motivated many works reporting advanced control strategies [2]–[6], some of them trying to overcome many problems of the classic PI speed control [7]. However, many of these controllers result in complex control laws that often lead to an impractical solution for engineering commissioning, which explains why the motor drive community and manufacturers have not been enthusiastic with these proposals [8]. Moreover, many of these control schemes focus on the round rotor motor case [6], [7], and [9]–[12] because considering the salient rotor case results in much more complex controllers (see [8] and [13], for instance).

Standard field-oriented control (FOC) is still the workhorse in industrial applications of PMSM because of its simplicity, i.e., easy commissioning, reliability, and good performance [14]–[16]. This control strategy is composed of two proportional-integral (PI) inner current loops and one outer PI speed loop [17]. However, this simple and successful idea has been employed in practice using intuitive ideas and, commonly, the formal design is intended to be performed using approximate linear models of the closed-loop system, which is nonlinear for the PMSM.

On the other hand, it is mentioned in [18] that although two-degree-of-freedom (2-DOF) control is perceived as obsolete, (see [19] for a recent approach that, however, is introduced for brushed dc motors), it constitutes an excellent option for robust speed control providing a practical solution for the electric drive community. In this respect, [20] and [21] proposed a 2-DOF control scheme that is intended for speed control in permanent magnet brushed dc motors. The reported experimental results are satisfactory in what concerns to closed-loop system robustness with respect to parameter uncertainties and external torque disturbances. However, as many of the 2-DOF controllers proposed in the literature, the design of control relies on neglecting the electric motor dynamics during the design and stability analysis, i.e., the PMSM dynamics is considered to be a simple first-order system [18], [22], [23]. We stress that it is important to perform controller design on the basis of a formal stability proof, which takes into account the electric dynamics because it is reasonable to wonder whether instability might appear if electrical dynamics are neglected [24], [25]. Moreover, in the widely recognized book [14], where passivity-based control is introduced for controller design in ac motors, is stated that another important reason to introduce a stability proof is to present tuning guidelines that replace intuition when designing

Manuscript received May 16, 2017; revised August 1, 2017, October 4, 2017, and November 3, 2017; accepted December 6, 2017. Date of publication January 8, 2018; date of current version April 2, 2018. The work of F. Mendoza-Mondragón was supported by CONACYT, México, under Grant 247771. *(Corresponding author: Víctor Manuel Hernández-Guzmán.)*

The authors are with the Facultad de Ingeniería, Universidad Autónoma de Querétaro, Centro Universitario, Cerro de las Campanas, Santiago de Querétaro 76010, México (e-mail: fmendoza@uaq.mx; vmhg@uaq.mx; juvenal@ieee.org).

Color versions of one or more of the figures in this paper are available online at http://ieeexplore.ieee.org.

Digital Object Identifier 10.1109/TIE.2017.2786203

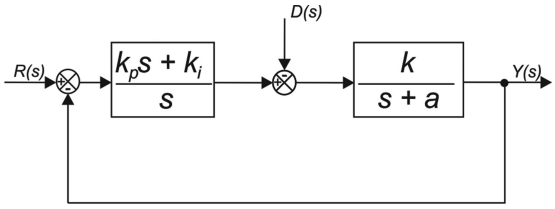

Fig. 1. Classical PI velocity control.

the controller. Motivated by the above arguments and the fact that PMSMs are nonlinear, it is important to extend to the case of PMSMs those controllers proposed in the literature under the assumption that motors have linear models.

In this paper, we extend the 2-DOF controller introduced in [21] and [22], to speed regulation in PMSM, and we validate the remarkable robustness properties of this controller with respect to parameter uncertainties and external torque disturbances. The complete control scheme is composed of two inner electric current loops driven PI controllers i.e., FOC, whereas a 2-DOF controller is designed for the motor mechanical subsystem. Our contribution is stated as follows. We take into account the nonlinear electric dynamics of the motor during the stability analysis; our control scheme is simple for practical implementation and it is valid for both motor cases: round and salient rotors. We formally prove global exponential stability of the desired equilibrium point; the stability conditions that we find are useful as tuning guidelines and they are intended to lead an easy commissioning. The robustness and simplicity of the 2-DOF controller make it suitable for commercial PMSM drives, as the examples in [26]. Finally, we present several experimental results that validate the performance of the proposed control system. Furthermore, experimental comparisons with classical PI speed control are also presented.

This paper is organized as follows. Tuning of classical PI velocity controllers is reviewed in Section II in order to motivate design of 2-DOF controllers. A previously introduced 2-DOF controller is reviewed in Section III. The PMSM model that we consider is presented in Section IV. Our main contribution is achieved in Section V. A study based on experiments is presented in Section VI in order to test performance of our proposal. Finally, some concluding remarks are given in Section VII.

II. Tuning of Classical PI Velocity Controllers

Consider the block diagram shown in Fig. 1, where a classical PI controller with gains k_p and k_i is used to control velocity in a first-order mechanical system. Notice that $k = 1/J$ and $a = B/J$, with J and B the system inertia and viscous friction coefficient, respectively. Closed-loop transfer function is given as follows (when $D(s) = 0$).

Suppose that it is desired that the closed-loop transient response be as that of a first-order system with a pole at $-1/\tau_r$ where τ_r is the desired closed-loop time constant. The two possibilities for root locus are presented in Fig. 2, which depend on the particular zero location $-k_i/k_p$. Black dots represent the considered closed-loop poles.

Consider the situation given in Fig. 2(a). In order to ensure a first-order closed-loop response with a pole at $-1/\tau_r$, i.e., the

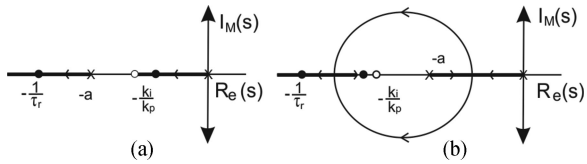

Fig. 2. Root locus diagrams for Fig. 1.

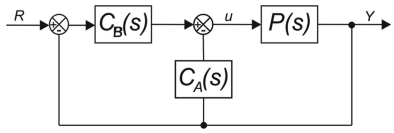

Fig. 3. Configuration of the 2-DOF robust controller.

closed-loop pole at the left, closed-loop pole at the right must cancel with zero at $-k_i/k_p$. If $-k_i/k_p$ is small, i.e., k_i is small, the closed-loop pole at the right is very close to zero. The effect of this pole cannot be canceled by any zero in the following transfer function:

$$\frac{Y(s)}{D(s)} = \frac{-ks}{s^2 + (a + kk_p)\, s + kk_i}$$

which represents the effect of disturbance $D(s)$, applied at the plant input on the system output $Y(s)$. Thus, rejection of this disturbance is very slow. Notice that if it is assumed that zero at $s = 0$ in the above transfer function cancels with the closed-loop pole at the right, then a nonzero steady state deviation due to disturbance would exist, which is not true as long as $k_i \neq 0$.

The integral gain k_i can be increased, i.e., for a faster disturbance rejection, as zero at $-k_i/k_p$ is assigned further to the left. Notice, however, that disturbance rejection performance is limited by the plant time constant if $a \geq k_i/k_p$. Hence, a satisfactory disturbance rejection performance is accomplished only if $a < k_i/k_p$. Thus, the situation in Fig. 2(b) must be considered. There, the two-real closed-loop poles are at the left of the open-loop zero at $-k_i/k_p$. Under this condition, according to [27, Lemma 8.3], overshoot is unavoidable, i.e., a first-order closed-loop transient response is not possible even when the closed-loop pole at the left is located at $-1/\tau_r$.

On the other hand, a slow disturbance rejection can also be improved by selecting two desired complex conjugated closed-loop poles, i.e., by specifying a closed-loop transient response exhibiting an overshoot, because this allows a larger ratio k_i/k_p [see Fig. 2(b)]. However, it is clear from Fig. 2(b) that, in such a case, there exists a closed-loop zero that cannot be canceled, which modifies the actual system response from that expected when specifying the complex conjugated poles.

Thus, it is concluded that classical PI control has a fundamental limitation: There is not a tuning rule that allows to simultaneously achieve desired transient responses when a desired velocity command is applied and when an external load disturbance is applied [28], Ch. 5. This motivates design of new control schemes such as 2-DOF controllers.

III. Two-Degrees-of-Freedom Controllers

According to the closed-loop configuration shown in Fig. 3, the following two-degrees-of-freedom controller

parameterization is proposed in [20] and [21] for robust permanent magnet brushed dc motor servo system:

$$C_A(s) = \frac{Q(s)}{P_n(s)\left(1 - Q(s)\right)}$$
$$C_B(s) = \frac{G_{ry}(s)}{\left(1 - G_{ry}(s)\right)}\left(\frac{1}{P_n(s)\left(1 - Q(s)\right)}\right)$$

where $P(s)$ and $P_n(s)$ represent, respectively, the actual plant and the nominal model of the plant that are used in the control design, $G_{ry}(s)$ is the desired model from the commanded input $R(s)$ to the actual output $Y(s)$, and $Q(s)$ is a filter that determines the robustness and the disturbance suppression performance. According to the methodology presented in [20] and [21] when $Q(s)$ is designed as the following Butterworth second-order filter:

$$Q(s) = \frac{1 + 1.41^2\tau_1 s}{1 + 1.41^2\tau_1 s + 1.41^2\tau_1^2 s^2}$$

and

$$P_n(s) = \frac{1}{J_n s + B_n},\ G_{ry}(s) = \frac{1}{\tau_r s + 1} \tag{1}$$

the following controller results

$$C_A(s) = \frac{J_n\left[1.41^2\tau_1 s^2 + \left(1 + \frac{B_n}{J_n}1.41^2\tau_1\right)s + \frac{B_n}{J_n}\right]}{1.41^2\tau_1^2 s^2} \tag{2}$$

where $J_n > 0$ and $B_n > 0$ represent the nominal motor inertia and viscous friction coefficient, respectively, $\tau_r > 0$ stands for the desired closed-loop system time constant, and $\tau_1 > 0$ is the fundamental parameter of $Q(s)$, which must be chosen to ensure the desired robustness and the disturbance suppression performance.

In this respect, the fact that the sensitivity function, i.e., a function that must be small to achieve robustness with respect to parameter uncertainties, and the transfer function from external disturbance to system output are proportional to factor $(1 - Q(s))$ is explained in [21]. Frequency response of this factor is that of a high-pass filter with zero gain at zero frequency whose corner frequency is close to $1/\tau_1$. Thus, better closed-loop system robustness properties with respect to both parameter uncertainties and external disturbances are achieved as $1/\tau_1$ is chosen larger than the bandwidth of the closed-loop system, i.e., $1/\tau_1 \gg 1/\tau_r$.

Finally, we stress that $P_n(s)$ given in (1) assumes torque is the plant input $U(s)$.

IV. PM Synchronous Motor Model

The standard DQ-model of a PMSM using Park transformation is given as

$$L_d\dot{I}_d = -R_s I_d + n_p L_q \omega I_q + v_d \tag{4}$$
$$L_q\dot{I}_q = -R_s I_q - n_p L_d \omega I_d - \Phi_M \omega + v_q \tag{5}$$
$$J\dot{\omega} = -b\omega + n_p\left(L_d - L_q\right)I_q I_d + \Phi_M I_q - T_L \tag{6}$$

where ω, J, b, and T_L stand for rotor speed, inertia, viscous friction coefficient, and the constant but unknown load torque, respectively. Expressions in (4) and (5) represent the electrical dynamics of the PMSM. Thus, v_d and v_q stand for the applied voltages, I_d and I_q are the electric currents defined correspondingly, whereas L_d, L_q, R_s, n_p and Φ_M are the positive constants representing, respectively, inductance, resistance, the number of pole pairs, and torque constant. Finally, $\tau_g = n_p(L_d - L_q)I_d I_q + \Phi_M I_q \in \mathcal{R}$ is the generated torque. The salient rotor case is obtained when $L_d \neq L_q$ and the round rotor case is obtained when $L_d = L_q = L$.

V. Robust Speed Servo System

Following Fig. 3, defining $R(s) = W^*(s) = \omega^*/s$ with ω^* a constant, $Y(s) = \omega(s)$, performing cancelations of powers of s, and applying the inverse Laplace transform, we find that the robust 2-DOF speed controller in (2) and (3), eq. (3) shown at the bottom of this page, can be written as

$$\begin{aligned} u = {} & k_p\tilde{\omega} + k_i\int_0^t \tilde{\omega}(r)dr + k_{ii}\int_0^t\int_0^r \tilde{\omega}(\sigma)d\sigma dr \\ & + k_{iii}\int_0^t\int_0^r\int_0^\sigma \tilde{\omega}(\upsilon)d\upsilon d\sigma dr - k_{pA}\omega \\ & - k_{iA}\int_0^t \omega(r)dr - k_{iiA}\int_0^t\int_0^r \omega(\sigma)d\sigma dr \end{aligned} \tag{7}$$

$$k_p = \frac{J_n}{\tau_r},\quad k_i = \frac{J_n\left(1.41^2\tau_1 + \frac{B_n}{J_n}1.41^2\tau_1^2\right)}{1.41^2\tau_1^2\tau_r}$$

$$k_{ii} = \frac{J_n\left(1 + \frac{B_n}{J_n}1.41^2\tau_1\right)}{1.41^2\tau_1^2\tau_r},\quad k_{iii} = \frac{B_n}{1.41^2\tau_1^2\tau_r},\ k_{pA} = \frac{J_n}{\tau_1}$$

$$k_{iA} = \frac{J_n\left(1 + \frac{B_n}{J_n}1.41^2\tau_1\right)}{1.41^2\tau_1^2},\quad k_{iiA} = \frac{B_n}{1.41^2\tau_1^2}$$

$$C_B(s) = \frac{J_n\left[1.41^2\tau_1^2 s^3 + \left(1.41^2\tau_1 + \frac{B_n}{J_n}1.41^2\tau_1^2\right)s^2 + \left(1 + \frac{B_n}{J_n}1.41^2\tau_1\right)s + \frac{B_n}{J_n}\right]}{1.41^2\tau_r\tau_1^2 s^3} \tag{3}$$

where $\tilde{\omega} = \omega^* - \omega$. It is not difficult to verify that the following expressions are equivalent to (7)

$$\begin{aligned} u =& \left(k_p + k_{pA}\right)\tilde{\omega} + \left(k_i + k_{iA}\right) z_1 + \left(k_{ii} + k_{iiA}\right) z_2 \\ &+ k_{iii} z_3 + T_L + b\omega^* \end{aligned} \tag{8}$$

$$z_1 = \int_0^t \tilde{\omega}(r)dr - \omega^* \frac{\alpha_1 k_{pA}}{k_i + k_{iA}}$$

$$z_2 = \int_0^t \left[\int_0^r \tilde{\omega}(\sigma)d\sigma - \omega^* \frac{\beta_2 k_{iA}}{k_{ii} + k_{iiA}} \right] dr - \omega^* \frac{\alpha_2 k_{pA}}{k_{ii} + k_{iiA}}$$

$$\begin{aligned} z_3 =& \int_0^t \left\{ \int_0^r \left[\int_0^\sigma \tilde{\omega}\left(\nu\right) d\upsilon - \omega^* \frac{k_{iiA}}{k_{iii}} \right] d\sigma - \omega^* \frac{\beta_1 k_{iA}}{k_{iii}} \right\} dr \\ &- \frac{b\omega^* + T_L}{k_{iii}} - \omega^* \frac{\alpha_3 k_{pA}}{k_{iii}} \end{aligned}$$

where $\alpha_1 > 0$, $\beta_2 > 0$, α_2, α_3, and β_1, are real constants such that $\alpha_1 + \alpha_2 + \alpha_3 = 1$ and $\beta_1 + \beta_2 = 1$. Moreover, we can write

$$\dot{z}_1 = \tilde{\omega},\ \dot{z}_2 = z_1,\ \dot{z}_3 = z_2 \tag{9}$$

if

$$\frac{\alpha_1 k_{pA}}{k_i + k_{iA}} = \frac{k_{iiA}}{k_{iii}} = \frac{\beta_2 k_{iA}}{k_{ii} + k_{iiA}}, \frac{\alpha_2 k_{pA}}{k_{ii} + k_{iiA}} = \frac{\beta_1 k_{iA}}{k_{iii}} \tag{10}$$

Hence, constants $\alpha_1, \alpha_2, \beta_1, \beta_2$ have to be chosen in order to satisfy these conditions. Now, consider the following controller:

$$v_d = -r_d I_d - n_p L_q \omega I_q - R_{di} \int_0^t I_d(t)dt \quad I_d^* = 0 \tag{11}$$

$$v_q = -r_q \rho - R_{qi} \int_0^t \rho(r)dr \qquad I_q^* = \frac{u}{\Phi_M} \tag{12}$$

where r_d, r_q, and R_{qi} are the positive constant scalars, and u is defined in (7), i.e., u is equivalent to (8). Adding and subtracting terms $b\omega^*$, $n_p(L_d - L_q)I_d I_q^*$, and $\Phi_M I_q^*$, using the second expression in (12), defining $\rho = I_q - I_q^*$, and using the fact that $\dot{\omega}^* = 0$, we can rewrite (6) as

$$\begin{aligned} J\dot{\tilde{\omega}} =& -\left(k_p + k_{pA} + b\right)\tilde{\omega} - \left(k_i + k_{iA}\right) z_1 - \left(k_{ii} + k_{iiA}\right) z_2 \\ &- k_{iii} z_3 - n_p \left(L_d - L_q\right) I_d \rho - n_p \left(L_d - L_q\right) I_d I_q^* \\ &- \Phi_M \rho \end{aligned} \tag{13}$$

which must be used along with (9). On the other hand, replacing (12), i.e., v_q, in (5), adding and subtracting terms $L_q \dot{I}_q^*$, $R_s I_q^*$, $\Phi_M \omega^*$, and $n_p L_d \omega^* I_d$, and using second expression in (12), we find

$$\begin{aligned} L_q \dot{\rho} =& -R_q \rho + n_p L_d \tilde{\omega} I_d - n_p L_d \omega^* I_d + \Phi_M \tilde{\omega} \\ &- \frac{L_q}{\Phi_M} [\left(k_p + k_{pA}\right)\dot{\tilde{\omega}} + \left(k_i + k_{iA}\right)\tilde{\omega} \\ &+ \left(k_{ii} + k_{iiA}\right) z_1 + k_{iii} z_2] - \frac{R_s}{\Phi_M} [\left(k_p + k_{pA}\right)\tilde{\omega} \\ &+ \left(k_i + k_{iA}\right) z_1 + \left(k_{ii} + k_{iiA}\right) z_2 + k_{iii} z_3] - R_{qi}\xi \end{aligned} \tag{14}$$

$$\xi = \int_0^t \rho(r)dr + \frac{\Phi_M \omega^*}{R_{qi}} + \frac{R_s \left(b\omega^* + T_L\right)}{\Phi_M R_{qi}} \tag{15}$$

where $R_q = r_q + R_s$. Finally, replacing (11) in (4) we have

$$\begin{aligned} L_d \dot{I}_d =& -\left(R_s + r_d\right) I_d - R_{di}\varphi \\ \dot{\varphi} =& I_d \end{aligned} \tag{16}$$

Hence, the closed-loop dynamics are given by (9) and (13)–(16). Note that (16) implies

$$\begin{aligned} |I_d(t)| \leq \left\|\left(\varphi(t), I_d(t)\right)\right\| \leq \alpha_1 \left\|\left(\varphi\left(0\right), I_d\left(0\right)\right)\right\| e^{-\lambda t} \\ \forall t \geq 0 \end{aligned} \tag{17}$$

For some constants $\alpha_1 > 0$, $\lambda > 0$, if $R_s + r_d > 0$, and $R_{di} > 0$. Thus, we only have to analyze stability of the dynamics (9) and (13)–(15), under condition (17). Defining the state of these dynamics as $x = [z_3, z_2, z_1, \tilde{\omega}, \xi, \rho]^T$, it is not difficult to realize that we can write (9) and (13)–(15) as

$$\dot{x} = A_1 x + A_2(x) I_d + A_3 I_d \tag{18}$$

where $A_3 \in \mathcal{R}^6$ is a constant vector, and $A_2(x) \in \mathcal{R}^6$ has the following entries:

$$A_2(4) = -\frac{n_p \left(L_d - L_q\right)}{J} \left(\rho + \frac{1}{\Phi_M}\sigma\right)$$

$$A_2(6) = \frac{n_p L_d \tilde{\omega}}{L_q} + \frac{n_p \left(L_d - L_q\right)\left(k_p + k_{pA}\right)\left(\rho + \sigma\right)}{\Phi_M J}$$

$$\begin{aligned} \sigma =& \left(k_p + k_{pA}\right)\tilde{\omega} + \left(k_i + k_{iA}\right) z_1 + \left(k_{ii} + k_{iiA}\right) z_2 \\ &+ k_{iii} z_3 \end{aligned}$$

and all the remaining entries are equal to zero. Notice that term $A_2(x)I_d$ contains the nonlinear terms arising from the motor model, which are bilinear and, hence, vector $A_2(x)$ is linear in x. Hence, it is clear that $\|A_2(x)\| \leq k_2\|x\|$ for some finite positive constant scalar k_2. Entries of matrix A_1 are zero excepting

$$\begin{aligned} A_1(4,1) =& -k_{iii}/J, \quad A_1(4,2) = -(k_{ii} + k_{iiA})/J \\ A_1(4,3) =& -\left(k_i + k_{iA}\right)/J, \\ A_1(4,4) =& -\left(k_p + k_{pA} + b\right)/J \\ A_1(4,6) =& -\Phi_M/J \\ A_1(6,1) =& ((k_p + k_{pA})/J - R_s/L_q)k_{iii}/\Phi_M \\ A_1(6,2) =& [((k_p + k_{pA})/J - R_s/L_q)(k_{ii} + k_{iiA}) - k_{iii}]/\Phi_M \\ A_1(6,3) =& [((k_p + k_{pA})/J - R_s/L_q)(k_i + k_{iA}) \\ &- (k_{ii} + k_{iiA})]/\Phi_M \\ A_1(6,4) =& [((k_p + k_{pA})(k_p + k_{pA} + b)/J \\ &- R_s(k_p + k_{pA})/L_q) - (k_i + k_{iA})]/\Phi_M + \Phi_M/L_q \\ A_1(6,5) =& -R_{qi}/L_q, \quad A_1(6,6) = (k_p + k_{pA})/J - R_q/L_q \\ A_1(1,2) =& A_1(2,3) = A_1(3,4) = A_1(5,6) = 1. \end{aligned} \tag{19}$$

Although (18) is a nonlinear differential equation, its solution is given as

$$x(t)=e^{A_1 t}x(0)+\int_0^t e^{A_1(t-\tau)}[A_2(x(\tau))I_d(\tau)+A_3 I_d(\tau)]d\tau.$$

This can be corroborated by differentiating the above solution to find $\dot{x}(t)$ and to verify that (18) is satisfied. See [29], Proof of Theorems 3 and 4, for an explanation on how to differentiate the integral above. This requires $A_2(x)I_d + A_3 I_d$ to be considered as the input of a linear system. See [30, (A4)] for a similar problem.

Assuming that matrix A_1 is Hurwitz, we have that $\|e^{A_1 t}\| \leq \gamma_1 e^{-\lambda_1 t}$, for some positive scalars γ_1, λ_1. Hence, taking the Euclidean norm on both sides, using (17) and $\|A_2(x)\| \leq k_2\|x\|$, and by direct integration of the term $\int_0^t \gamma_1 e^{A_1(t-\tau)}\|A_3\|\|I_d(\tau)|d\tau$ we find that

$$\begin{aligned}\|x(t)\|\, e^{\lambda_1 t} \leq{}& \gamma_1\,\|x(0)\| \\ &+\frac{\gamma_1\,\|A_3\|}{\lambda-\lambda_1}\alpha_1\,\|\varphi(0),I_d(0)\|\left(e^{-\lambda_1 t}-e^{-\lambda t}\right)e^{\lambda_1 t} \\ &+\int_0^t \gamma_1\left[k_2\alpha_1\,\|\varphi(0),I_d(0)\|\,e^{-\lambda\tau}\right] \\ &\times\|x(\tau)\|\,e^{\lambda_1\tau}d\tau\end{aligned}$$

Using the Gronwall–Bellman inequality [31, Appendix A], we find that

$$\begin{aligned}\|x(t)\| \leq{}& \gamma_1\,\|x(0)\|\,e^{-\lambda_1 t} \\ &+\frac{\gamma_1\,\|A_3\|}{\lambda-\lambda_1}\alpha_1\,\|\varphi(0),I_d(0)\|\left(e^{-\lambda_1 t}-e^{-\lambda t}\right) \\ &+B(t)e^{-\lambda_1 t}e^{\gamma_1 k_2\alpha_1\|\varphi(0),\ \ I_d(0)\|/\lambda} \qquad (20)\end{aligned}$$

$$\begin{aligned}B(t)={}&\frac{\gamma_1^2 k_2\,\|x(0)\|\,\alpha_1\,\|\varphi(0),I_d(0)\|}{-\lambda}\left(e^{-\lambda t}-1\right) \\ &-\frac{\gamma_1^2\,\|A_3\|\,k_2[\alpha_1\,\|\varphi(0),I_d(0)\|]^2}{\lambda-\lambda_1} \\ &\times\left(\frac{e^{-\lambda t}-1}{\lambda}-\frac{e^{-(2\lambda-\lambda_1)t}-1}{2\lambda-\lambda_1}\right).\end{aligned}$$

Note that $\frac{1}{\lambda-\lambda_1}(e^{-\lambda_1 t}-e^{-\lambda t})>0$, for all $t>0, \lambda>0, \lambda_1>0$, and converges exponentially to zero as time grows. Reviewing the procedure followed to obtain (20), we can verify that $B(t)>0$, for all $t\geq 0$, because $\frac{1}{\lambda-\lambda_1}(e^{-\lambda_1 t}-e^{-\lambda t})>0$. From (20), we conclude that $x(t)$ converges globally and exponentially to zero if $\lambda>0$ and $\lambda_1>0$. This completes the proof of the following proposition, which constitutes our main contribution.

Proposition 1: Consider the dynamic model (4)–(6) in a closed loop with the controller (7), (11), and (12). The whole state of the closed-loop system, i.e., $x=[z_3,z_2,z_1,\tilde{\omega},\xi,\rho]^T$ and I_d, φ, converges globally and exponentially to zero if matrix A_1, defined in (20), is Hurwitz, $R_s+r_d>0$, $R_{di}>0$ and conditions in (10) are satisfied. Controller gains must be chosen such that these conditions are satisfied.

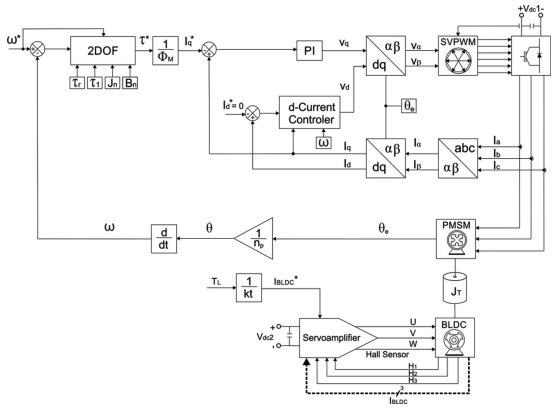

Fig. 4. Block diagram of the test-bed configuration.

Remark 1: It is not difficult to verify that, using (7)

$$\frac{k_{iiA}}{k_{iii}}=\tau_r\approx\frac{k_{iA}}{k_{ii}+k_{iiA}}=\frac{J_n\left(1+\frac{B_n}{J_n}1.41^2\tau_1\right)}{\frac{J_n\left(1+\frac{B_n}{J_n}1.41^2\tau_1\right)}{\tau_r}+B_n}$$

If B_n is small, which is common in practice, the first condition in (10) is satisfied using some $\beta_2>1$ close to unity, and because $\beta_1+\beta_2=1$, second condition in (10) has to be satisfied using some $\beta_1<0$ and some $\alpha_2<0$. Hence, we have to choose an (possibly large) $\alpha_1>0$ satisfying the first condition in (10), which requires a (possibly negative) real constant α_3 to satisfy $\alpha_1+\alpha_2+\alpha_3=1$. We stress that once both conditions in (10) be evaluated, all of the constants $\beta_1,\beta_2,\alpha_1,\alpha_2,\alpha_3$ are exactly known.

VI. Experimental Result

In this section, the performance of the control scheme introduced in this paper, designated from now on as the 2-DOF speed controller, is evaluated. A comparison study is also presented, when a classical PI controller replaces the 2-DOF speed controller in the outer loop, intended to regulate velocity, and two identical classical PI electric current controllers are used. When using the 2-DOF velocity controller, expressions in (11) and (12) are employed. Fig. 4 shows the block diagram of the experimental setup. The PMSM model Estun EMJ-04APB22 is the motor to be controlled. A brushless dc (BLDC) motor model Hurst DMA020402B101 is used to apply external step torque disturbances at the PMSM shaft. The BLDC motor is controlled using the servo amplifier B15A8 from the advanced motion controls. Also, the shaft coupling of both motors includes a mass to increase the inertia of the whole system. Hence, inertia uncertainties can be introduced when required.

Controllers to be tested were implemented in the Texas Instruments development kit TMDSHVMTRPFCKIT, with a microcontroller TMS320F28335. Integral operations involved in these controllers were numerically calculated using the trapezoidal method. Notice that the proposed controller given in (7) leads to implementation issues such as iterated integral overflow. Nevertheless, this problem is avoided using the equivalent

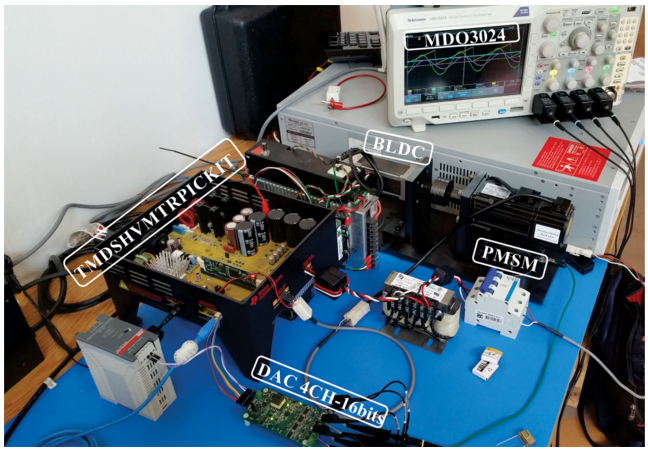

Fig. 5. Experimental setup.

TABLE I
NOMINAL PARAMETERS OF THE PMSM MODEL ESTUN EMJ-04APB22

Variable	Value
Rated power	400 W
Rated phase current	2.7 A_{rms}
Rated phase to phase voltage	200 V_{rms}
Rated speed	3000 r/min
Rated torque	1.27 N·m
Encoder resolution	10 000 counts/rev
Number of poles pairs (n_p)	4
Stator winding resistance (R_s)	2.7 Ω
Stator inductance $(L = L_d = L_q)$	8.5 mH
Torque constant (Φ_M)	0.301 N·m/A
Flux linkage (k_e)	0.0615 Wb
Nominal inertia (J)	31.69e^{-6} kg· m^2
Nominal viscous friction (b)	52.79e^{-6} N·m· s/rad
Nominal static friction (c)	0.0289 N·m

TABLE II
TEST-BED PARAMETERS

Variable	Value	
Total inertia (J_T)	167.1e^{-6} kg·m^2	5.2 J
Total viscous friction (b_T)	106.9e^{-6} N·m·s/rad	2b
Total static friction (c_T)	0.0384 N·m	1.32c

expression in (8). Sampling period used to control the motor electric currents I_q and I_d was 100 μs whereas sampling period used to control speed was 500 μs. Variables were measured using a 16-b digital–analog converter card with four channels. These values were updated every 100 μs and collected by a Tektronix MDO3024 oscilloscope (see the experimental setup in Fig. 5).

The PMSM nominal parameters are shown in Table I. In order to evaluate the effectiveness of the 2-DOF speed controller, the PMSM was tested under several conditions such as speed regulation, torque disturbance rejection, and parameter variations. The BLDC coupled motor is used to increase the nominal parameters and to introduce torque disturbances. When the BLDC motor is coupled to the PMSM, the shaft parameters change to those as shown in Table II. We designate these parameters as the test-bed parameters. Notice that the most critical parameter, i.e., inertia, changes more than five times and the viscous friction coefficient increases two times when the BLDC motor is coupled to the PMSM shaft. We also include unmodeled parameters, such as the static friction.

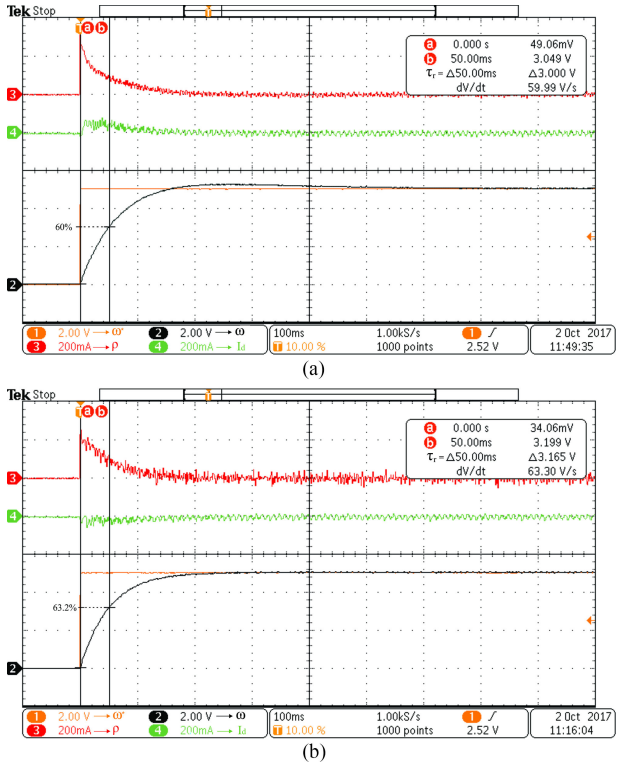

Fig. 6. Experimental response to a step speed command under nominal conditions. (a) PI controller. (b) 2-DOF controller.

A. Step Speed Command

In this test, speed control was performed under nominal conditions given in Table I, i.e., PMSM is controlled without coupling the BLDC motor to its shaft. The desired closed-loop time response is set to be of first order with a time constant of 50 ms. The commanded speed step magnitude was $\omega^* = 1500$ r/min. The resulting responses are shown in Fig. 6. The desired speed and measured speed ω^* and ω are indicated with the orange and black traces, respectively, with a scaling factor of 3000 r/min/10 V. This speed scaling factor is used in all the reported experiments. The red and green traces indicate the I_q current error (ρ) and the I_d current error, respectively, with a scaling factor of 1 A/1 V. This electric current scaling factor is used in all the reported experiments, also the color traces.

It is verified that the measured speed at $\Delta t = 50$ m is 63.2% of ω^* for the 2-DOF controller and a little bit lower when the classical PI controller is used. This was the best tuning achieved empirically for the classical PI velocity controller following ideas in Section II, i.e., by choosing a small ratio $k_{i\omega}/k_{p\omega}$ compared to $1/\tau_r$. Thus, both controllers respond as desired in this test. However, the real performance improvement achieved by the 2-DOF controller will be observed in the next experiments

TABLE III
CONTROLLER PARAMETERS

2-DOF speed controller					
	τ_r	τ_1	Φ_M	J_n	B_n
	50 ms	1.8 ms	0.301	$31.69e^{-6}$	$52.79e^{-6}$
PI speed controller					
		$k_{p\omega}$	$k_{i\omega}$		
		0.0038	0.02		
I_q and I_d current controller					
	r_d	r_q	R_{di}		R_{qi}
PI	60	60	6000		6000
2-DOF	60	60	6000		6000

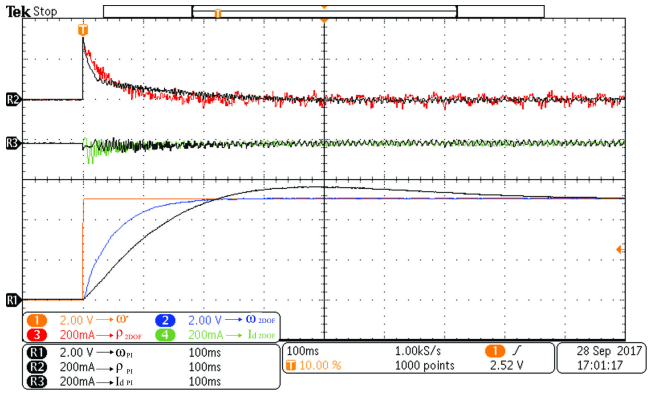

Fig. 7. Experimental result of the step response of the PI and the 2-DOF controller under an inertia change.

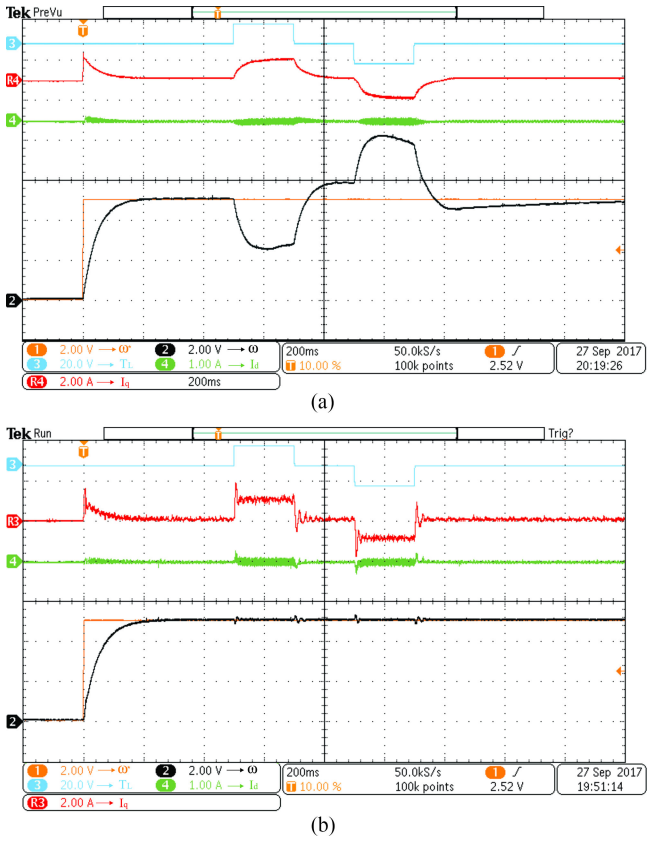

Fig. 8. Experimental results of the step response under parameter variation and load disturbance. (a) PI controller. (b) 2-DOF controller.

when parameter uncertainties and external load disturbances appear. Parameters of controllers are shown in Table III. In the case of the 2-DOF speed controller, parameters in Table III were checked to satisfy all the stability conditions in established in Proposition 1. Notice that all the controller gains can be computed from the parameters in Table III. Parameter τ_1 was chosen using the criterion in the last paragraph of Section III, i.e., $1/\tau_1 \gg 1/\tau_r$. Also remark that $J_n = J$ and $B_n = b$.

B. Robustness to Inertia Variation

In this test, the BLDC motor was coupled to the PMSM shaft in order to increase inertia to $J_T = 5.2$ J. The BLDC motor was not used to generate any torque. Also notice that, as explained above, this also modifies the other test-bed parameters shown in Table II. Gains in Table III, i.e., those used in the previous experiments, were used again for both controllers. As it is observed in Fig. 7, the 2-DOF controller (blue trace) still gives the same desired transient and steady state responses. This proves robustness with respect to inertia changes. Although the use of PI velocity controller (black trace) results in a rise time that is similar to the settling time achieved with the 2-DOF controller, an overshoot is produced that renders the settling time larger achieved with the PI velocity controller.

Although there are many works in the literature that overcome the problem of inertia changes with complex solutions such as online inertia estimation or adaptive controllers [7], [32], the reported experimental results in [4], [5], [7], and [33] consider changes of less than three times the nominal inertia. In this respect, note that the results obtained in this paper with a 2-DOF controller considers change of five times the nominal inertia providing a simple and effective manner to address this problem.

C. Robustness to Motor Parameters Variation and Load Disturbances

In this test, the BLDC motor is coupled to the PMSM shaft. Thus, test-bed parameters have changed to those shown in Table II, i.e., the motor will be tested under inertia, viscous friction, and static friction variations and, also, step torque load disturbances will be applied. Parameters of the 2-DOF controller are kept the same as in Table III, in order to verify the robustness of this controller. On the other hand, the PI controller gains have been adjusted to $k_{p\omega} = 0.14$ and $k_{i\omega} = 0.15$ in order to achieve the 50-ms time constant again. This has been done to render fair comparison, since it is clear that the new test-bed parameters, shown in Table II, require new PI controller gains to achieve the same time constant. In this test, the BLDC motor applies torque disturbances of +/–0.25 N·m (cyan trace, with a torque scaling factor of 0.25 N·m/10 V, as in all the reported experiments) at a steady state.

Fig. 8(a) shows response with the PI speed controller. As we can see, the speed regulation is deteriorated by torque disturbances. Although the PI controller can accomplish the desired

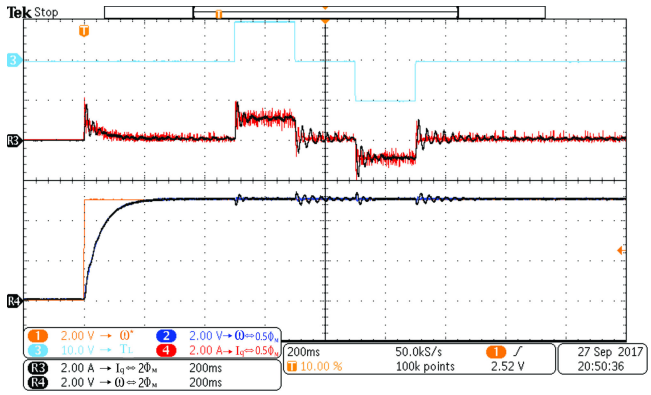

Fig. 9. Step response of the 2-DOF with an over- and underestimated torque constant.

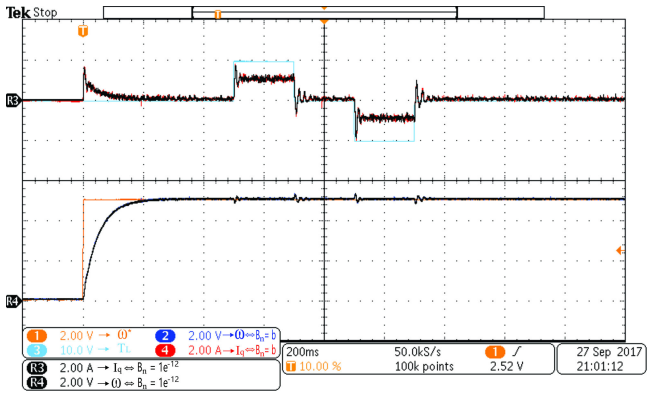

Fig. 10. Step response and disturbance rejection of the 2-DOF when B_n is considered close to zero.

transient response, it is not capable to achieve a good disturbance rejection. On the other hand, response with the 2-DOF controller is shown in Fig. 8(b). As we can see, parameter variations do not affect the desired time response and torque disturbances are rejected very fast. Notice that the parameter variations that we have considered are larger than the parameter variations reported in previous experimental results [7]. From Figs. 7 and 8, we conclude that the 2-DOF controller is more robust than the classical PI controller with respect to parameter uncertainties and load disturbances. Additionally, regardless of the desired speed reference, the transient response is also preserved, this property, known as the nominal performance recovery, is studied in [34] for ac machines. However, the (nonlinear) electric dynamics of the ac machine is not taken into account.

D. Mismatch of the Nominal Torque Constant

From (12), we can see that the 2-DOF controller output is directly related to the knowledge of the motor torque constant. However, in practice, this constant may not be accurately known, or it might be affected by temperature changes during the normal motor operation. Fig. 9 shows the speed response to a commanded step speed change under parameter changes and torque disturbance, i.e., when the BLDC motor is coupled to the PMSM shaft. Black trace represents the response when torque constant is assumed to be two times the nominal torque constant, whereas blue trace represents the response when torque constant is assumed to be of half the nominal torque constant. Observe that transient response is preserved, however, response to external torque disturbances presents oscillations due to overestimation of torque constant. This behavior can be attributed to the fact that for a higher value of the torque constant the commanded current is lower and this decreases the robustness of the controller. However, as remarked in [35], an increase in the temperature leads to a lower generated torque by the PMSM. Notice that, in such a case, the 2-DOF speed controller still gives the desired transient response with an excellent robustness to load changes.

E. Underestimated Viscous Friction

As we can see in (7), viscous friction is another parameter required to compute the 2-DOF controller gains. However, in practice, viscous friction is a value that rarely appears in the motor nameplate. In Fig. 10, speed response is presented when controller gains are computed assuming that $B_n = 1.0^{-12}$ and all of the other parameters in Table III remain the same. Notice that B_n cannot be zero. In this test, the BLDC motor is coupled to the PMSM shaft to introduce some step torque disturbances. We realize that the obtained response is almost identical to the response in Fig. 8(b), i.e., when all of the parameters in Table III are used. This proves that the 2-DOF controller is robust to the uncertainty in the viscous friction coefficient.

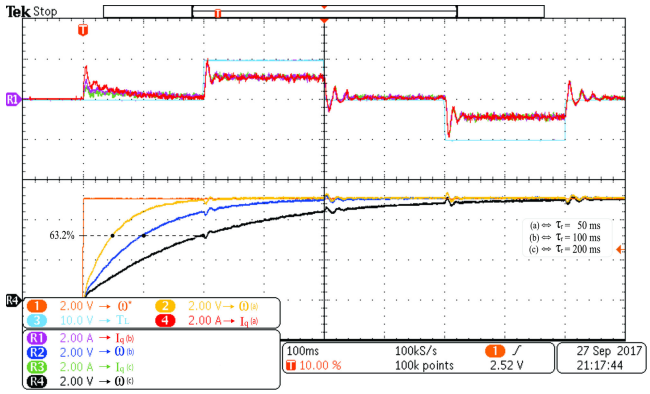

Fig. 11. Disturbance rejection when different time constants are employed.

F. Changes in the Desired Time Constant

Finally, the 2-DOF controller is tested when different desired time constants are required in the presence of external torque disturbances. As we can see in Fig. 11, the desired transient response is decoupled from the disturbance rejection performance. According to this and all of the above results, a simple tuning procedure is followed as: Choose the desired time constant (τ_r), consider an approximate inertia (J_n), use very small (≈ 0) viscous friction coefficient (B_n), and choose a desired robustness performance (τ_1) such that $1/\tau_1 \gg 1/\tau_r$. Hence, simplicity in selection of the controller parameters is an important advantage of 2-DOF control with respect to classical PI speed control where transient response is coupled to disturbance rejection performance. We remark that 2-DOF controller, as the PI

controller, can be tuned using two main parameters (J_n, τ_1 and $k_{p\omega}$, $k_{i\omega}$ respectively). However, the 2-DOF parameters have a clear physical interpretation making the tuning easier for engineering commissioning, notice that τ_r is considered a free parameter not a tuning gain.

VII. Conclusion

In this paper, we presented a two-degrees-of-freedom controller for speed regulation in PMSM. Our proposal extends a previously introduced controller for permanent magnet brushed dc motors to the case of PMSM. The control scheme that we propose includes two internal electric current loops driven by proportional and PI controllers, i.e., FOC of PMSM. Our main contribution is that the nonlinear electrical dynamics of the PMSM is taken into account during the stability analysis and we formally prove global exponential stability. The resulting controller offers a simple and effective control strategy for adjustable speed in PMSM drives. The resulting stability conditions provide a practical tuning guideline for the main parameters J_n and τ_1. It is worth mentioning that time constant τ_r can be chosen independently of the desired robustness τ_1. Performance achieved is tested through several experiments where a comparison with the classical PI speed controller is also presented. Although parameters of the proposed controller depend on the nominal parameters of the motor, the closed-loop system is robust with respect to parameter uncertainties and external torque disturbances. Moreover, a superior performance is observed when compared with classical PI speed control. An important contribution of our proposal is that it constitutes a simple controller that is valid for both classes of PMSM: the round and salient rotor cases. Future research will focus on the position regulation and trajectory tracking.

Acknowledgment

The work of F. Mendoza-Mondragón is encouraged by his beloved wife Maria Ruth. He also thanks, Laboratorio de Investigación en Control Reconfigurable (LICORE, A.C.), México, for allowing him to use its facilities and valuable advice.

References

[1] J. Linares-Flores, C. Garcia-Rodriguez, H. Sira-Ramirez, and O. D. Ramirez-Cardenas, "Robust backstepping tracking controller for low-speed PMSM positioning system: Design, analysis, and implementation," *IEEE Trans. Ind. Informat.*, vol. 11, no. 5, pp. 1130–1141, Oct. 2015.

[2] T. D. Do, H. H. Choi, and J.-W. Jung, "θ-D approximation technique for nonlinear optimal speed control design of surface-mounted PMSM drives," *IEEE/ASME Trans. Mechatronics*, vol. 20, no. 4, pp. 1822–1831, Aug. 2015.

[3] D. Q. Dang, M. S. Rafaq, H. H. Choi, and J.-W. Jung, "Online parameter estimation technique for adaptive control applications of interior PM synchronous motor drives," *IEEE Trans. Ind. Electron.*, vol. 63, no. 3, pp. 1438–1449, Mar. 2016.

[4] Y.-S. Choi, H. H. Choi, and J.-W. Jung, "Feedback linearization direct torque control with reduced torque and flux ripples for IPMSM drives," *IEEE Trans. Power Electron.*, vol. 31, no. 5, pp. 3728–3737, May 2016.

[5] T. D. Do, H. H. Choi, and J.-W. Jung, "Nonlinear optimal DTC design and stability analysis for interior permanent magnet synchronous motor drives," *IEEE/ASME Trans. Mechatronics*, vol. 20, no. 6, pp. 2716–2725, Dec. 2015.

[6] T. Tarczewski and L. M. Grzesiak, "Constrained state feedback speed control of PMSM based on model predictive approach," *IEEE Trans. Ind. Electron.*, vol. 63, no. 6, pp. 3867–3875, Jun. 2016.

[7] J. Jung, V. Q. Leu, T. D. Do, E. Kim, and H. H. Choi, "Adaptive PID speed control design for permanent magnet synchronous motor drives," *IEEE Trans. Power Electron.*, vol. 30, no. 2, pp. 900–908, Feb. 2015.

[8] V. Petrovic, R. Ortega, and A. M. Stankovic, "Interconnection and damping assignment approach to control of PM synchronous motors," *IEEE Trans. Control Syst. Technol.*, vol. 9, no. 6, pp. 811–820, Nov. 2001.

[9] K. Belda and D. Vosmik, "Explicit generalized predictive control of speed and position of PMSM drives," *IEEE Trans. Ind. Electron.*, vol. 63, no. 6, pp. 3889–3896, Jun. 2016.

[10] S. Kim, J.-S. Lee, and K. Lee, "Offset-free robust adaptive back-stepping speed control for uncertain permanent magnet synchronous motor," *IEEE Trans. Power Electron.*, vol. 31, no. 10, pp. 7065–7076, Oct. 2016.

[11] M. Siami, D. A. Khaburi, A. Abbaszadeh, and J. Rodriguez, "Robustness improvement of predictive current control using prediction error correction for permanent-magnet synchronous machines," *IEEE Trans. Ind. Electron.*, vol. 63, no. 6, pp. 3458–3466, Jun. 2016.

[12] S.-K. Kim, K.-G. Lee, and K.-B. Lee, "Singularity-free adaptive speed tracking control for uncertain permanent magnet synchronous motor," *IEEE Trans. Power Electron.*, vol. 31, no. 2, pp. 1692–1701, Feb. 2016.

[13] A. Donaire and S. Junco, "On the addition of integral action to port-controlled Hamiltonian systems," *Automatica*, vol. 45, no. 8, pp. 1910–1916, Aug. 2009.

[14] R. Ortega, A. Loría, P. J. Nicklasson, and H. Sira-Ramírez, *Passivity-Based Control of Euler-Lagrange Systems*. London, U.K.: Springer London, 1998.

[15] F. Mendoza-Mondragón, V. M. Hernández-Guzmán, and R. V. Carrillo-Serrano, "Velocity regulation in PMSMs using standard field oriented control plus adaptation," *Asian J. Control*, vol. 17, no. 6, pp. 2382–2388, Nov. 2015.

[16] S. Li and Z. Liu, "Adaptive speed control for permanent-magnet synchronous motor system with variations of load inertia," *IEEE Trans. Ind. Electron.*, vol. 56, no. 8, pp. 3050–3059, Aug. 2009.

[17] V. M. Hernández-Guzmán and R. Silva-Ortigoza, "PI control plus electric current loops for PM synchronous motors," *IEEE Trans. Control Syst. Technol.*, vol. 19, no. 4, pp. 868–873, Jul. 2011.

[18] L. Harnefors, S. E. Saarakkala, and M. Hinkkanen, "Speed control of electrical drives using classical control methods," *IEEE Trans. Ind. Appl.*, vol. 49, no. 2, pp. 889–898, Mar/Apr. 2013.

[19] Y. I. Son, I. H. Kim, D. S. Choi, and H. Shim, "Robust cascade control of electric motor drives using dual reduced-order PI observer," *IEEE Trans. Ind. Electron.*, vol. 62, no. 6, pp. 3672–3682, Jun. 2015.

[20] T. Umeno and Y. Hori, "Robust speed control of DC servomotors using modern two degrees-of-freedom controller design," *IEEE Trans. Ind. Electron.*, vol. 38, no. 5, pp. 363–368, Oct. 1991.

[21] T. T. Umeno and Y. Hori, "Robust DC servosystem design based on the parametrization of two degrees-of-freedom control systems," in *Proc. Annu. Conf. IEEE Ind. Electron. Soc.*, 1989, vol. 2, pp. 313–318.

[22] W. Chuen-Gan and L. Qiu, "Robust two degree of freedom regulators for velocity ripple elimination of AC permanent magnet motors," in *Proc. IEEE Int. Conf. Control Appl.*, 2000, pp. 156–161.

[23] C. Xia, B. Ji, T. Shi, and Y. Yan, "Two-degree-of-freedom proportional integral speed control of electrical drives with Kalman-filter-based speed estimation," *IET Elect. Power Appl.*, vol. 10, no. 1, pp. 18–24, Jan. 2016.

[24] T.-J. Tarn, A. K. Bejczy, X. Yun, and Z. Li, "Effect of motor dynamics on nonlinear feedback robot arm control," *IEEE Trans. Robot. Autom.*, vol. 7, no. 1, pp. 114–122, 1991.

[25] R. V. Carrillo-Serrano, V. M. Hernández-Guzmán, and V. Santibáñez, "Global asymptotic stability of PD control for PM stepper motor servo-systems," *Asian J. Control*, vol. 14, no. 5, pp. 1449–1457, Sep. 2012.

[26] J. Yang, W. -H. Chen, S. Li, L. Guo, and Y. Yan, "Disturbance/uncertainty estimation and attenuation techniques in PMSM drives—A survey," *IEEE Trans. Ind. Electron.*, vol. 64, no. 4, pp. 3273–3285, Apr. 2017.

[27] G. C. Goodwin, S. F. Graebe, and M. E. Salgado, *Control System Design*. Upper Saddle River, NJ, USA: Prentice-Hall, 2001.

[28] V. M. Hernández-Guzmán, R. Silva-Ortigoza, and R. V. Carrillo-Serrano, *Automatic Control: Design Theory, Prototype Construction, Modeling, Identification and Experimental Tests*. (In Spanish). México City, México: Colección CIDETEC-IPN, 2013.

[29] C.-T. Chen, *Linear System Theory and Design*. New York, NY, USA: Holt, Rinehart Winston, 1984.
[30] S. Peresada and A. Tonielli, "High-performance robust speed-flux tracking controller for induction motor," *Int. J. Adapt. Control Signal Process.*, vol. 14, pp. 177–200, 2000.
[31] H. K. Khalil, *Nonlinear Systems*. Upper Saddle River, NJ, USA: Prentice-Hall, 2002.
[32] L. Niu, D. Xu, M. Yang, X. Gui, and Z. Liu, "On-line inertia identification algorithm for PI parameters optimization in speed loop," *IEEE Trans. Power Electron.*, vol. 30, no. 2, pp. 849–859, Feb. 2015.
[33] A. Formentini, A. Trentin, M. Marchesoni, P. Zanchetta, and P. Wheeler, "Speed finite control set model predictive control of a PMSM fed by matrix converter," *IEEE Trans. Ind. Electron.*, vol. 62, no. 11, pp. 6786–6796, Nov. 2015.
[34] R. Errouissi, A. Al-Durra, and S. M. Muyeen, "Experimental validation of a novel PI speed controller for AC motor drives with improved transient performances," *IEEE Trans. Control Syst. Technol.*, early access, Jun. 2017, doi: 10.1109/TCST.2017.2707404.
[35] D. D. Reigosa, D. Fernandez, T. Tanimoto, T. Kato, and F. Briz, "Permanent-magnet temperature distribution estimation in permanent-magnet synchronous machines using back electromotive force harmonics," *IEEE Trans. Ind. Appl.*, vol. 52, no. 4, pp. 3093–3103, Jul. 2016.

Fortino Mendoza-Mondragón received the M.S. degree in automatic control and instrumentation in 2012, from Universidad Autónoma de Querétaro, Santiago de Querétaro, México, where he is currently working toward the Ph.D. degree in electrical engineering, AC motor drives.

His research interests include modeling, parameter identification, electric machine drives, and power conversion systems for renewable energy sources.

Víctor Manuel Hernández-Guzmán was born in Santiago de Querétaro, México. He received the B.S. degrees from Instituto Tecnológico de Querétaro, Santiago de Querétaro, México, the M.S. degree from Instituto Tecnológico de la Laguna, Torreón, México, and the Ph.D. degree from CINVESTAV-IPN, México City, México, in 1988, 1991, and 2003, respectively, all in electrical engineering.

Since 1995, he has been a Professor with Universidad Autónoma de Querétaro, where he currently teaches classical and nonlinear control. He is a coauthor of the book *Automatic Control: Design Theory, Prototype Construction, Modelling, Identification and Experimental Test* (in Spanish) (México City, México: Colección CIDETEC-IPN, 2013).

Juvenal Rodríguez-Reséndiz (SM'13) He received the B.S., M.S. and Ph.D. degrees in electrical engineering from Queretaro State University, México, in 2004, 2007 and 2010, respectively.

He has been a Professor with Querétaro State University, Querétaro, México, since 2008. He has worked on industrial automation projects for 15 years. He is currently the Chair of the Engineering Automation Program and Master in automation with Querétaro State University. He is with the Mexican Academy of Sciences, the National Research Academy, México, and seven associations regarding engineering issues.

Prof. Rodríguez-Reséndiz is the IEEE Querétaro Section President. He was the recipient of different awards for his developments regarding education technology.